Influence of interband transitions on electron–phonon coupling measurements in Ni films

Patrick E. Hopkins, J. Michael Klopf, and Pamela M. Norris

The reduction in size and the increase in speed of opto- and magnetoelectronic devices is making the probability of nonequilibrium electron–phonon phenomena greater, leading to increased thermal resistance in these devices. The measurement of electron–phonon coupling in materials in these devices is becoming increasingly important for accurate thermal management. Here femtosecond thermoreflectance is used to measure the electron–phonon coupling factor in thin Ni films of varying thickness grown on Si and glass substrates. The thermoreflectance response is measured at 1.3 and 1.55 eV, yielding drastically different responses due to the Fermi-level transition at 1.3 eV in Ni. The influence of this transition on the thermoreflectance response results in a measurement of the electron–phonon coupling factor that is twice as high as that recorded in previous measurements that were unaffected by the Fermi-level transition.

OCIS codes: 120.5700, 160.3380, 240.0310, 260.2160, 260.3060, 310.6860.

1. Introduction

Understanding the ultrafast dynamics of electrons in microelectronic devices composed of thin-film metal systems is important in a wide range of applications. Examples include hot electron photochemistry of atoms or molecules adsorbed on solid surfaces,[1] laser ablation and processing of metals,[2] highly reflective mirrors used in laser systems,[3] and development of field effect transistors (i.e., metal-semiconductor field-effect transistors) used in microwave devices.[4] As the speeds of these devices increase, the advent of a nonequilibrium in temperature between the electrons and the lattice becomes more probable, creating an increase in the thermal resistance in the device. With the miniaturization trend of these devices comes the need to accurately measure these nonequilibrium processes for accurate thermal management.

The rate of electron–phonon equilibration, governed by the electron–phonon coupling factor, G, has been measured with the transient thermoreflectance (TTR) technique on a variety of metal films.[2,5–11] The TTR technique employs a pump–probe laser setup to monitor the transient electron response to a pump pulse that is incident on the surface of the thin-film sample.[3,9] The change in reflectance as a result of the pump pulse is monitored by a weaker probe pulse. Depending on the energy of the pump and probe, the monitored changes in reflectance could be attributable to inter- and/or intraband transitions. This change in reflectance is first related to the change in electron and/or lattice temperature using a thermoreflectance model, and these temperatures are then used in conjunction with an appropriate thermal model to determine G. Traditionally, when the resulting TTR response is dominated by interband transitions, G has been successfully determined by assuming a thermoreflectance model in which the TTR response is directly related to the electron temperature.

Several previous works have focused on electron–phonon coupling measurements at energies for which the resulting TTR response has varying contributions from interband transitions.[8,11–14] Sun *et al.*,[13] Fatti *et al.*,[14] and Eesley[12] studied the TTR response of Au, Ag, and Cu films, respectively, at the lowest energy d band (relative to the Fermi energy) to Fermi surface transition. At the interband transition threshold (ITT), the magnitude of the TTR response increases significantly from the magnitude of the off-ITT response. In addition, the TTR effects of this transition

P. E. Hopkins and P. M. Norris (pamela@virginia.edu) are with the Department of Mechanical and Aerospace Engineering, University of Virginia, P.O. Box 400746, Charlottesville, Virginia 22904-4746, USA. J. M. Klopf is with the Free Electron Laser Facility, Jefferson Laboratory, 12000 Jefferson Avenue, MS 18, Newport News, Virginia 23606, USA.

Received 6 September 2006; revised 10 November 2006; accepted 16 November 2006; posted 30 November 2006 (Doc. ID 74834); published 20 March 2007.

0003-6935/07/112076-08$15.00/0

are detectable in the energy range of the Fermi smearing around the ITT. Smith and Norris[11] studied the electron–phonon coupling in Au films at electron energies far below the ITT; i.e., only electrons undergoing intraband transitions participated in the electron–phonon energy transfer. Hohlfeld *et al.*[8] studied the electron–phonon coupling in Au of various thicknesses at energies at and around the ITT, and measured the same rate of electron–phonon coupling as Smith and Norris.[11] In Au it is apparent that the large TTR response associated with the ITT does not affect the electron–phonon coupling measurements.

Previous studies have focused on the noble metals due to their relatively simplified band structure compared with transition metals. Noble metals have a very distinct, high-energy ITT since the *s*-band–*d*-band crossing is significantly lower than the Fermi level. Therefore the first allowable *d*-band to available *s*-band transition is very large for Cu (2.15 eV), Au (2.4 eV), and Ag (4 eV) making it easy to isolate the effects of the ITT on thermoreflectance and hence on the G measurements.[12] However, transition metals pose a greater problem in examining the effects of the ITT on determining G through TTR since characteristically their band structures are shifted from the noble metals so the *s*-band–*d*-band crossing is at or above the Fermi level. This produces several allowable low-energy *d*-band (d_1-band) to *s*-band transitions making it difficult to examine the effects of the ITT. For example, Cr has Fermi transitions at 0.8 (ITT), 1.0, 1.4, and 1.6 eV, W has transitions at 0.85 (ITT), 1.6, and 1.75 eV,[15] and Ni has transitions at 0.25 (ITT), 0.4, and 1.3 eV.[16] These low-energy transitions make it possible to examine the effects of higher-energy *d*-band to Fermi-level transitions (not the ITT) on the TTR response and the resulting value of G as determined using the traditional procedure.

The aim of this paper is to examine the TTR response and the subsequent G measurement on Ni films at the 1.3 eV sub-*d*-band to Fermi-level transition. Detailed band calculations for Ni are available in the references.[16–20] Weiling and Callaway[19] recalculated the band structure of Ni but were careful to note that the aim of their calculations was to rectify the discrepancies in band calculations away from the Fermi surface. The most widely accepted low-energy Fermi surface transitions for Ni are those calculated through thermoreflectance results by Hanus *et al.*[16] Their data result in the three Fermi surface transitions previously mentioned, with the 0.4 eV transition occurring in the minority spin band (spin down), and the 0.25 and 1.3 eV transitions occurring in the majority spin band (spin up). However, due to Fermi smearing at room temperature, the termination sites in the flat *d* band above the Fermi level would be occupied, therefore inhibiting the 0.4 eV spin-down transition from the sub-*d* band. In addition, since the 0.25 eV spin-up transition is so much less than the 1.3 eV transition, the 1.3 eV transition can be studied with no interference from the large thermoreflectance response that would be associated with the lower-energy transitions.

This band splitting of the Ni energy levels is characteristic of all ferromagnetic materials below the Curie temperature. The band structure of ferromagnetic Ni is considered a juxtaposition of the band structure of nonferromagnetic Ni and Cu at a point in k space with energy removed from the Fermi energy; the nonferromagnetic Ni structure consists of the spin-up electrons, and the Cu structure represents the shifted structure of the spin-down electrons.[17] Because of this, ferromagnetic Ni also exhibits a splitting of the Fermi level. Since the transition of interest is the 1.3 eV sub-*d*-band (d_2-band) to the Fermi-level (*s*-band) transition in the spin-up bands, any potential demagnetization to the resulting nonferromagnetic Ni structure will not affect this transition. However, care is still taken in the experimental procedure to remain below the Curie temperature.

This paper presents the measurements of G in 30, 40, and 50 nm thick Ni films on Si and soda glass (primarily composed of SiO_2) substrates at energies dominated by inter- and intraband transitions. Nickel films have been of interest lately, particularly the relation of the magnetization to the electron dynamics.[6,21–24] Before electron relaxation, demagnetization has been observed[6,23] with the majority of the magnetization recovered during the first few picoseconds when electron cooling is primarily attributable to electron–phonon coupling.[24] Clearly a more coherent view of electron–phonon thermalization measurements will benefit the studies of spin dynamics and magnetization.

2. Thermal and Reflectance Models

The laser heating of metals can be described by three time intervals, which are thoroughly described in the references.[8,25] The earliest of the time intervals, the relaxation time, τ_{ee}, represents the time is takes the excited electrons to relax into a Fermi distribution through e–e collisions and is typically of the order of 10 fs for metals at room temperature.[3,26] The ballistic transport of the electrons also occurs during this time, and the depth to which the electrons ballistically travel is significantly larger than the optical penetration depth in noble metals.[2,8,27] After relaxation occurs in the electron system, the higher-temperature electrons transmit energy to the lattice through the electron–phonon scattering processes as the electrons conduct energy deeper into the film away from the optically excited region.[27,28] The electron–phonon interactions eventually lead to the two subsystems reaching an equilibrium temperature within a time governed by both the specific heats of the systems and the electron–phonon coupling factor.[9] This thermalization time, τ_{ep}, is typically of the order of 1 ps for metals. This time is dependent upon the carrier density in the optical penetration depth, which is substrate dependent,[27] and is inversely related to G.[27,29,30]

The nonequilibrium temperature induced in TTR experiments with laser pulse durations longer than τ_{ee} but shorter than τ_{ep} can be accurately predicted with the parabolic two-step (PTS) model.[26,31] This model, given in the following equations, describes the

rate of energy exchange between the electrons and phonons in a metal film:

$$C_e(T_e)\frac{\partial T_e}{\partial t} = \frac{\partial}{\partial x}\left(k_e(T_e,\ T_l)\frac{\partial T_e}{\partial x}\right) - G(T_e - T_l) + S(x,\ t), \tag{1}$$

$$C_l\frac{\partial T_l}{\partial t} = G(T_e - T_l). \tag{2}$$

In Eq. (1), the electron thermal conductivity can be estimated as $k_e(T_e, T_l) = k_{eq}[T_e/T_l]$, where k_{eq} is the thermal conductivity at room temperature.[26] This term assumes that electron–phonon collisions dominate the energy transfer,[32] which is valid for temperatures far below the Fermi temperature.[33] The electron heat capacity is expressed as $C_e(T_e) = \gamma_e T_e$,[34] although over the predicted electron temperatures achieved in the study reported here, C_e can be estimated as a constant.[29] The term in the PTS model used to describe the incident laser pulse is given by

$$S(x,\ t) = 0.94\ \frac{(1-R)}{t_p\delta}\ J\ \exp\left[-\frac{x}{\delta} - 2.77\left(\frac{t}{t_p}\right)^2\right], \tag{3}$$

where the reflectivity, R, and the energy penetration depth, δ, are material properties, while the fluence, J, and the pulse duration, t_p, are parameters of the incident laser pulse. Here, δ can be used to describe the sum of the radiation and ballistic penetration depths. In Ni, however, the ballistic transport is negligible so the ballistic effects are not considered,[2,8,33] and therefore the incident energy is assumed to be deposited a distance of 14.3 nm into the film, the optical penetration depth in Ni at the incident laser wavelength, 800 nm.[35,36] Since the films examined in this study have thicknesses of 30 nm and greater, it is valid to assume that the source term neglects any interaction with the substrate that would require a modification to Eq. (3).[8] This is further justified by calculating the reflectance of a thin Ni film for an absorbing film on a nonabsorbing substrate.[37] The results of these calculations for Ni films on Si and SiO_2 substrates are shown in Fig. 1. The reflectance for films 30 nm and thicker is approximately equal to the reflectance calculated for a bulk material, 68%, justifying the assumption that film thickness will not affect the absorbed energy density.

In TTR experiments, it is the change in reflectivity resulting from a change in temperature in the sample that is measured. The change in reflectance of a metal can be related to the change in temperature through the complex dielectric function, $\Delta\varepsilon(\omega, \Delta T) = \Delta\varepsilon_1(\omega, \Delta T) + i\Delta\varepsilon_2(\omega, \Delta T)$.[38] For ultrashort pulses ($\tau_{ee} < t_p < \tau_{ep}$), the resulting reflectance, and thus the dielectric function, is a function of both ΔT_e and ΔT_l and can be expressed as $\Delta\varepsilon(\omega, \Delta T_e, \Delta T_l) = \Delta\varepsilon_1(\omega, \Delta T_e, \Delta T_l) + i\Delta\varepsilon_2(\omega, \Delta T_e, \Delta T_l)$. For small changes in temperature, ($\Delta T < 100$ K) , $\Delta\varepsilon$ can be expressed as a linear change in ΔT_e and ΔT_l as[9,39,40]

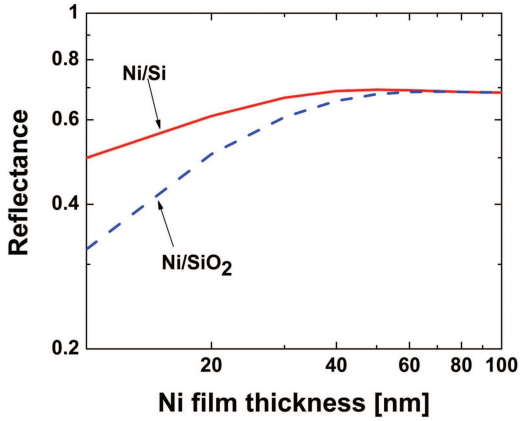

Fig. 1. (Color online) Reflectance off the surface of a Ni film on both Si and SiO_2 substrates as a function of film thickness at a probing wavelength of 800 nm calculated with the equations developed by Abeles (Ref. 37). For films thinner than 30 nm, the reflectance deviates by more than 10% from the bulk reflectance, indicating that for films in this range the absorbed laser energy in TTR experiments could be affected by the underlying substrate.

$$\Delta\varepsilon = \Delta\varepsilon_1 + i\Delta\varepsilon_2 = \frac{\partial\varepsilon_1}{\partial T_e}\Delta T_e + \frac{\partial\varepsilon_1}{\partial T_l}\Delta T_l + i\left(\frac{\partial\varepsilon_2}{\partial T_e}\Delta T_e + \frac{\partial\varepsilon_2}{\partial T_l}\Delta T_l\right). \tag{4}$$

The change in reflectance in TTR experiments can be related to the dielectric functions by[41]

$$\frac{\Delta R}{R} = \frac{1}{R}\left[\frac{\partial R}{\partial\varepsilon_1}\Delta\varepsilon_1 + \frac{\partial R}{\partial\varepsilon_2}\Delta\varepsilon_2\right]. \tag{5}$$

By plugging Eq. (4) into Eq. (5), the reflectance can be simplified to the familiar thermoreflectance equation[9,39]

$$\frac{\Delta R}{R} = a\Delta T_e + b\Delta T_l, \tag{6}$$

where $a \propto \partial R/\partial T_e$, and $b \propto \partial R/\partial T_l$. This reflectance model directly relates the change in reflectance in the TTR experiments to the electron and lattice temperatures in the PTS model. Once the change in temperature of the electron and lattice systems is known, this information can be used to determine thermophysical properties such as the thermal conductivity or the electron–phonon coupling constant [Eqs. (1) and (2)].[35]

3. Experimental Details

Six Ni samples of various thicknesses were made on Si and glass substrates. The Si substrates were 480 μm thick with ⟨100⟩ orientation and n type doped with Ph. The glass substrates were Corning 0211 borosilicate cover glass, 200 μm thick, and ~70% SiO_2. The Ni samples were fabricated in a high-vacuum (low 10^{-6} Torr) in-house sputtering system with a 99.995% pure Ni target. Before being intro-

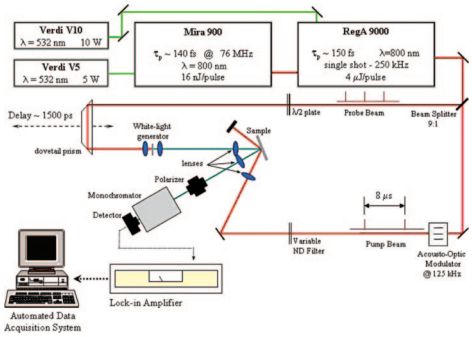

Fig. 2. (Color online) TTR experimental setup.

duced into the sputtering chamber, the substrates were spin cleaned with reagent alcohol (90.7% ethyl alcohol, 4.8% isopropyl alcohol, 4.5% methyl alcohol, and 0.12% water), trichloroethylene, and methanol, then baked for 5 min at 120 °C to remove any residual water vapor, and then put in an O_2 plasma line cleaner for 10 min for further cleaning and oxide removal. This cleaning process was immediately followed by placing the substrates into the deposition chamber. The Ni was deposited at a 600 V bias and ~15 mTorr Ar. This was calibrated to ~5.5 nm/min by depositing onto a Si wafer partially covered with a glass slide, then measuring the step height with a Tencor surface profiler. A portion of every sample was covered in this fashion, and the Ni thicknesses of 30, 40, and 50 nm were validated to within 1 nm with the profiler.

The TTR data were taken with the pump–probe experimental setup shown in Fig. 2. The primary output of the laser system emanates from a Coherent RegA 9000 amplifier operating at a 250 kHz repetition rate with approximately 4 μJ per pulse and a 150 fs pulse width at 800 nm (1.55 eV). The pulses were split at a 9:1 pump-to-probe ratio when using 800 nm for the pump and probe. The pump beam, modulated at 125 kHz by an acousto-optic modulator (AOM), was focused down to a 100 μm radius spot size to achieve 5 J m^{-2} fluence. The probe beam was focused to the center of the pump beam on the Ni interface to achieve a pump-to-probe fluence ratio of 10:1. The radii of the pump and probe beams were measured with a sweeping knife edge, and the phase of the reflectance was used for data correction, as outlined in the references.[42]

There is enough energy per pulse from the RegA amplifier to generate a white-light continuum when the ultrashort laser pulse is focused in pure single crystal sapphire. This white-light generation relies on Kerr self-focusing and self-phase modulation (SPM), which ensures that the continuum generated is emitted in the same polarization and has the same temporal characteristics as the high-power incident pulse.[43] It is important that the pulse compression stage of the RegA amplifier be properly aligned to maintain a pulse width of 150 fs and a close to ideal Gaussian temporal shape. The pulse width and shape were monitored with an Inrad 5-14B autocorrleator that was modified to suit the relatively low repetition rate RegA amplifier system.

The spectral bandwidth of the white-light continuum pulses ranges from the IR to the blue part of the visible spectrum. Although the continuum pulses have the same temporal structure as the input pulses, as the pulses propagate through the sapphire crystal and subsequent achromatic lenses, the dispersion of these materials will broaden the pulse resulting in different wavelengths arriving at the sample surface at slightly different times. Since the TTR measurements and the resolution of G depend on the temporal decay of the reflectance, the relative delay of the probe with respect to the pump is needed, not the absolute delay. Where the absolute delay of the probe with respect to the pump changes based on probe wavelength attributable to pulse broadening, the relative delay is consistently defined between data as the time delay after the peak probe reflectance (t_0).

By generating the white-light pulses from the probe path, probing at 948 nm (1.3 eV) was achieved. A slightly altered setup was used in this situation. The beam splitter that regulates the pump and probe relative powers was reversed from the former case, so that the RegA pulses were split at a 9:1 probe:pump ratio; this ensured that the pulses focused in the sapphire crystal had sufficient power to generate white light. The beam exiting the crystal was then sent through an 800 nm high reflector (HR), which was necessary to reject the 800 nm fundamental wavelength that remained at an average power of approximately 700 mW, far exceeding the 2.3 mW average power of the white-light spectrum remaining after the HR. The probe beam was then focused to the center of the pump beam and reflected through an Oriel 777250 monochromator to select the 948 nm wavelength.

The fluence of the pump was chosen to allow less than a 100 K rise in the electron system temperature to ensure the validity of the linear reflectance model.[9,11] Assuming that all the incident energy that is not reflected off the sample surface is absorbed in the film ($A = 1 - R$), the maximum temperature rise in the series of films is approximately 60 K for the 30 nm Ni film on glass substrate as calculated by simple equations for predicting maximum electron temperature.[8] Since the substrates used in the study are considered nonabsorbing ($n_{2\_Si} = 0.0065$ and $n_{2\_SiO_2} = 0$, where n_2 is the imaginary part of the complex index of refraction representing the relative amount of absorption by the material),[44] $A = 1 - R$ can be assumed. This electron temperature change also ensures that the electron temperature is below the Curie temperature of Ni (630 K)[45]; therefore there should be no demagnetization effects of the electronic band structure, although this should not be an issue since the TTR response will be dominated by the transitions in the spin-up band, as mentioned in Section 1.[46]

The low repetition rate of the RegA system and the one-shot-on–one-shot-off modulation rate of the

pump beam ensures minimal residual heating between pump pulses. However, valuable information about the electronic processes must still be extracted from the phase of the data through phase correction techniques.[42] At 1.3 eV, the TTR response is dominated by the electron response from the interband transition. Therefore the peak increase attributable to the high temperature electrons is orders of magnitude higher than the negative reflectance response of Ni during electron–phonon equilibrium. However, at 1.55 eV, which is off the interband reflectance peak, the increase attributable to the high-temperature electrons is significantly smaller, and of the same order of magnitude as the equilibrium negative response.

The phase change of the raw data gives valuable information about the electron response. The phase of the signal is a sinusoidal function that is defined relative to the phase of the pump that is controlled by the AOM.[42] A shift in the phase of the measured probe reflectance of 180° from the peak response represents a reflectance that is opposite in sign (negative) but with the same magnitude as the peak response. The observed phase changes for the 30 nm Ni/Si sample at 1.3 and 1.55 eV probe energies are presented along with the phase-corrected reflectance data in Figs. 3(a) and 3(b). The phase of the pump was set to zero so that when the probe was in phase with the pump at t_0, thus yielding the peak probe response, the phase was defined as 0°. As seen in Figs. 3(a) and 3(b), the peak TTR response corresponds to the zero phase.

After the peak reflectance, different phase responses were observed at 1.3 and 1.55 eV during the time when the majority of the electron–phonon coupling occurred (~2 ps after the peak). The phase of the 1.3 eV response [Fig. 3(a)] shifted ~100° once electron–phonon equilibrium was achieved resulting in a signal that was opposite in phase and only a fraction of the magnitude of the signal at the point of the peak electron response. Note that a change in phase of exactly 90° corresponds to a zero reflectance response. Since the peak TTR response for Ni when probing at 1.3 eV (which corresponds to the interband transition) is so large, the strong positive reflectance response at this probe energy arising from the nonequilibrium heating dominates the equilibrium TTR response, which has negative magnitude. However, in the 1.55 eV TTR data, the nonequilibrium response characteristic of the 1.3 eV transition is significantly smaller since the probe energy is removed from the interband transition energy. The peak nonequilibrium TTR response is almost the same value as the equilibrium reflectance response of Ni; correspondingly, the phase shift is almost 180° (~165°). Note that the data were taken with the same pump fluence, so the change in electron temperature once the electrons and phonons reach equilibrium is the same for both probe energy measurements; this is evident by the value of the reflectance at ~4 ps after the electron peak once the electrons and phonons have equilibrated.

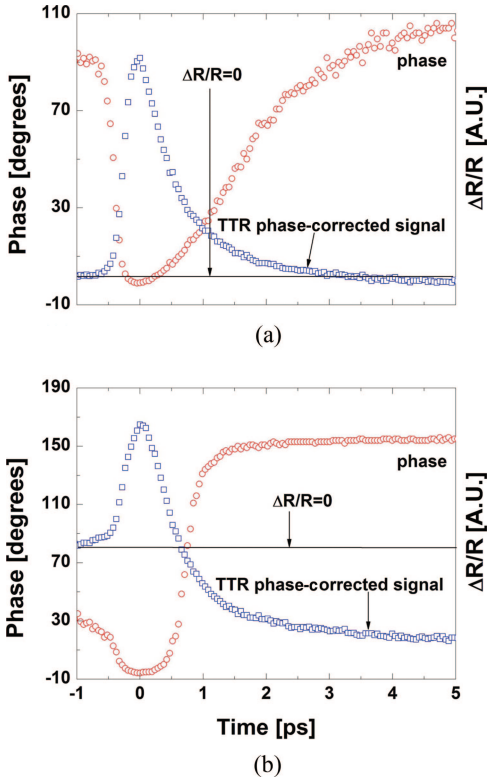

Fig. 3. (Color online) Observed phase and phase-corrected reflectance data on the 30 nm Ni/Si sample at a probe energy of (a) 1.3 and (b) 1.55 eV. The phase of the pump was set to zero so that when the probe was in phase with the pump at t_0, thus yielding the peak probe response; the phase was defined as 0°. (a) At a probe energy of 1.3 eV, the signal after the interband response is ~90° out of phase with the pump, which is evident from the phase-corrected data that have a magnitude that is only a small fraction of the peak value at t_0. (b) However, at a probe energy of 1.55 eV, the signal after the interband response is almost 180° out of phase with the pump, and therefore the phase corrected data are approximately the magnitude, but opposite in sign to the value at t_0.

Figure 4 compares the phase-corrected data of the 30 nm Ni/Si sample at the two probe energies. Note the large differences in the magnitudes and durations of the positive electron TTR responses between the 1.3 and 1.55 eV probes. The duration of the positive TTR response is much longer when probing at 1.3 eV than at 1.55 eV. In the inset of Fig. 4, the peak of the 1.3 eV data is scaled down by a factor of 40 to match the peak of the 1.55 eV data. Note that after the effect of the interband transition on the TTR data, the data relax to the same equilibrium response: -4×10^{-4} at ~4 ps after the peak. This large increase in the TTR response at the 1.3 eV probe energy, which is associated with the Fermi-level transition, will be shown to affect G measurements by significantly dominating the nonequilibrium response. It is this nonequilibirum response owing to the electrons undergoing intraband transitions that is used to determine G.

4. Results

The data from the six Ni samples at the two probe energies were fit with Eqs. (1) and (2) using the values

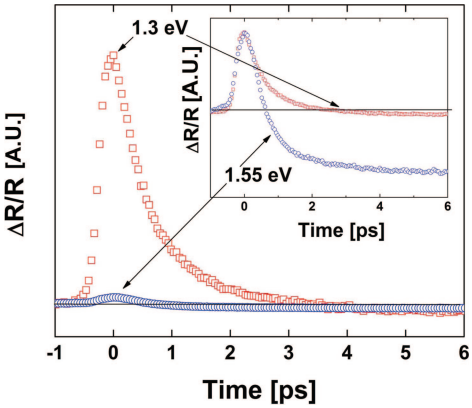

Fig. 4. (Color online) Comparison of the TTR response at probe energies of 1.3 and 1.55 eV. The influence of the interband transition on the 1.3 eV data is apparent by the value of the maximum peak, which is significantly greater than that observed in the 1.55 eV probe data since the probe is removed from the 1.3 eV interband transition. The effect of this transition on the TTR response lasts much longer at 1.3 eV than at 1.55 eV. At both probe energies, the TTR response relaxes to a negative response after the interband positive peak, and both signals reach the same value when the electrons and phonons come to equilibrium. The inset shows the 1.3 eV data scaled to the peak of the 1.55 eV data by dividing the 1.3 eV data by a factor of 40.

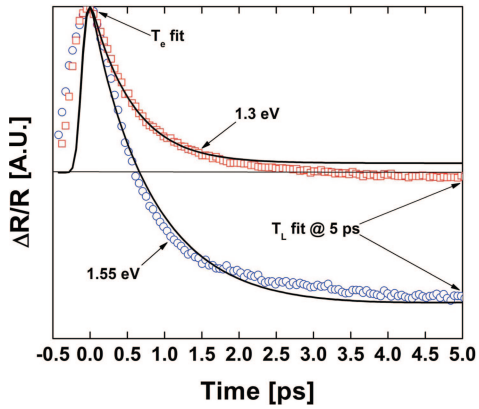

Fig. 5. (Color online) PTS model fit to the 1.3 and 1.55 eV data on the 30 nm Ni/Si film with the reflectance model, Eq. (6). The model was fit to the first 1.0 ps of data following the electron peak. The PTS electron temperature was fit to the peak, and the lattice temperature was fit to the point 5.0 ps after the peak. The data in this graph are normalized at the peak value.

for reflectance calculated in Fig. 1 and the thermophysical constants found in the references.[34,36] The thermal conductivity, k_{eq}, was assumed to be reduced from the bulk value and different for each film thickness. This was calculated by relating the reduced electrical resistivity to the reduced conductivity at each film thickness assuming the Weidmann–Franz law. The electrical resistivity film to bulk ratios of 1.85, 1.8, and 1.7 were determined on Ni films,[47] which were related to reduced conductivity values of 49.1, 50, and 53.5 W m^{-1} K^{-1} for the 30, 40, and 50 nm films, respectively. Equations (1) and (2) were solved using the Crank–Nicolson method.[29] Once the predicted temperature profiles were determined, the PTS model was fit to the TTR data via Eq. (6) iterating on the value of G until a least-squares minimum error was achieved in the first 1.0 ps after the electron peak. The coefficient a was determined by fitting the peak of the electron temperature profile in the PTS model to the peak of the TTR data at t_0, and the coefficient b was determined by fitting the lattice temperature profile 5 ps after the electron peak when the electron and lattice temperatures were equal. This is the standard procedure that has been used in the past to accurately determine G from TTR data.[9,39]

The PTS model fitted to the 30 nm Ni/Si data at the two probe energies is shown in Fig. 5. The best fit Gs for this sample at 1.3 and 1.55 eV were 5.8×10^{17} and 3.7×10^{17} W m^{-3} K^{-1}, respectively. The ratio a/b resulting from the best fit G during the fitting procedure was -3.3 for the 1.3 eV data and -0.08 for the 1.55 eV data—intuitive since the peak at 1.3 eV is so much greater than the 1.55 eV peak. These ratios remained within 10% for every sample at each probe energy. Since a was so much larger than b for the 1.3 eV data, the resulting reflectance model from the sum of the PTS temperature profiles resembles the electron temperature profile. This results in a model that does not fit the data well outside of 2.0 ps after the electron peak. However, since G was determined in the first 1.0 ps after the peak, this should not be an issue for determining the rate of electron–phonon coupling. In addition, since the lattice profile contributes so little to this temperature profile, the reflectance model essentially reduces down to $\Delta R/R = a\Delta T_e$. This is the same reflectance model used by several groups to determine the G in Au films around the interband transition energy.[8,10] These groups measured the same G at these energies with this model as Smith and Norris[11] measured at energies far below the ITT with their intraband reflectance model.

Figure 6 presents the results for the G measurements as functions of film thickness. The circles represent the values of G measured on the Ni/Si samples, and the squares represent the measurements on the Ni/glass samples. The values of G determined from the 1.3 eV data were consistently higher, by almost 100%, than those determined for the 1.55 eV data. The average value of G determined from the 1.55 eV data (3.55×10^{17} W m^{-3} K^{-1}) is in good agreement with the value determined by Wellersoff *et al.*[2,48] at a 3.11 eV pump and probe energy (3.6×10^{17} W m^{-3} K^{-1}). Neither the 1.55 nor the 3.11 eV energies are close enough to an interband Fermi surface transition to induce the large increase in the TTR response seen in the 1.3 eV data in this study, and an accurate determination of the thermophysical property G was possible. However, the large TTR response seen in this study at 1.3 eV resulted in an overprediction of G outside the range of experimental error. This could be a result of a large nonlinear TTR response associated with probing very close to the d_2-band to Fermi-level transition, causing

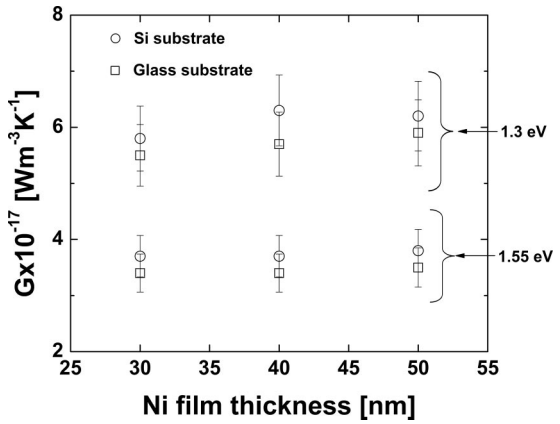

Fig. 6. Electron–phonon coupling factor measurements as a function of film thickness. The measurement of G was consistently higher at 1.3 eV probe energy than at 1.55 eV. The average value of G determined from the 1.55 eV data agreed well with the past value reported at 3.11 eV (Refs. 2 and 48). In addition, a slight difference in measurements is observed between the Ni/Si samples and the Ni/glass samples, which could be due to substrate effects resulting in an increased temperature in the film by inhibiting thermal diffusion across the film–substrate interface.

the reflectance model $\Delta R/R = a\Delta T_e$ to break down. However, this model was successfully used for determining G in Au at the ITT (d_1-band to Fermi-level transition). This indicates that at higher-energy d-band to Fermi-level transitions, measurements of G made using the linear reflectance model are affected by the large TTR response.

At each energy, the value of G determined on the Ni/Si sample was higher than that determined on the Ni/glass sample. Note, however, that the values were within 10% of each other at each film thickness, which was the error associated with the experimental measurements and fitting routine. Although within the experimental error, this slight deviation may be explained by the energy density present in the film during the electron–phonon coupling process. As the highly energetic nonequilibrium electrons couple with the lattice in the probed region on the surface of the film, the electrons are also traveling out of the probed region and diffusing through the film at a rate dictated by k_{eq}. As the electron energy density decreases, the time it takes for the electrons and phonons to equilibrate decreases, and therefore G increases. As the electrons travel to the film–substrate interface, they are more likely to lose energy to a highly conductive substrate (Si) than to an insulating substrate (glass). This same type of relationship was shown for NiFe films on Si and glass substrates.[27] Therefore the electron temperatures would be slightly lower in the Ni/Si films than in the Ni/glass films because of increased conductance across the film–substrate interface in the Ni/Si samples. This suggests that the value of G measured on the Ni films in this study could be an electron-temperature-dependent property, which was analytically shown in the case of Au films.[49]

5. Conclusions

This paper measured the electron–phonon coupling factor, G, in 30, 40, and 50 nm thick Ni films grown on Si and glass substrates with the pump–probe TTR technique. Measurements were taken at probe energies of 1.3 and 1.55 eV. Ni has a d_2-band to Fermi-level transition at 1.3 eV, so the TTR response at 1.3 eV shows a large positive increase during electron–phonon coupling that was associated with the interband reflectance response. The measurement of G when the interband response dominated the data resulted in a value of G that was almost 100% larger than the measurement taken at energies removed from an interband transition. However, previous studies have shown that the TTR response attributable to the d_1-band to Fermi-level transition (i.e., at the ITT) does not affect G measurements in Au using the same reflectance model. This suggests that the higher-energy (non-ITT) transitions could affect electron–phonon coupling measurements by yielding a large TTR response that cannot be taken into account by conventional thermoreflectance models. More TTR experiments need to be performed on well-characterized metals (i.e., Au) to examine the effects of these sub-d-band to Fermi-level transitions. This study also showed evidence that G could be an electron-temperature-dependent thermophysical property. However, this specific conclusion needs to be studied in greater detail by measuring G at different fluences and on thinner films where the electron system temperature could be drastically affected by substrate conductivity and film thickness.

This work was funded through National Science Foundation grant CTS-0536744. The authors thank Rich Salaway and Jenni Simmons for insightful discussions and critical reading of the manuscript. Patrick Hopkins acknowledges the financial support from the National Science Foundation through the Graduate Research Fellowship Program.

References

1. J. W. Gadzuk, "Resonance-assisted hot electron femtochemistry at surfaces," Phys. Rev. Lett. **76,** 4234–4237 (1996).
2. S.-S. Wellershoff, J. Hohlfeld, J. Gudde, and E. Matthias, "The role of electron–phonon coupling in femtosecond laser damage of metals," Appl. Phys. A. **69,** Suppl. S99–S107 (1999).
3. T. Q. Qiu and C. L. Tien, "Femtosecond laser heating of multilayer metals—I. Analysis," Int. J. Heat Mass Transfer **37,** 2789–2797 (1994).
4. A. Majumdar, K. Fushinobu, and K. Hijikata, "Effect of gate voltage on hot-electron and hot-phonon interaction and transport in a submicrometer transistor," J. Appl. Phys. **77,** 6686–6694 (1995).
5. J. L. Hostetler, A. N. Smith, D. M. Czajkowsky, and P. M. Norris, "Measurement of the electron–phonon coupling factor dependence on film thickness and grain size in Au, Cr, and Al," Appl. Opt. **38,** 3614–3620 (1999).
6. J. Hohlfeld, E. Matthias, R. Knorren, and K. H. Bennemann, "Nonequilibrium magnetization dynamics of nickel," Phys. Rev. Lett. **78,** 4861–4864 (1997).
7. J. Hohlfeld, J. G. Muller, S.-S. Wellershoff, and E. Matthias, "Time-resolved thermoreflectivity of thin gold films and its

dependence on film thickness," Appl. Phys. B **64,** 387–390 (1997).
8. J. Hohlfeld, S.-S. Wellershoff, J. Gudde, U. Conrad, V. Jahnke, and E. Matthias, "Electron and lattice dynamics following optical excitation of metals," Chem. Phys. **251,** 237–258 (2000).
9. P. M. Norris, A. P. Caffrey, R. J. Stevens, J. M. Klopf, J. T. McLeskey, and A. N. Smith, "Femtosecond pump–probe nondestructive examination of materials," Rev. Sci. Instrum. **74,** 400–406 (2003).
10. T. Q. Qiu, T. Juhasz, C. Suarez, W. E. Bron, and C. L. Tien, "Femtosecond laser heating of multilayer metals—II. Experiments," Int. J. Heat Mass Transfer **37,** 2799–2808 (1994).
11. A. N. Smith and P. M. Norris, "Influence of intraband transitions on the electron thermoreflectance response of metals," Appl. Phys. Lett. **78,** 1240–1242 (2001).
12. G. L. Eesley, "Generation of nonequilibrium electron and lattice temepratures in copper by picosecond laser pulses," Phys. Rev. B **33,** 2144–2151 (1986).
13. C. K. Sun, F. Vallee, L. Acioli, E. P. Ippen, and J. G. Fujimoto, "Femtosecond-tunable measurement of electron thermalization in gold," Phys. Rev. B **50,** 15337–15348 (1994).
14. N. D. Fatti, C. Voisin, M. Achermann, S. Tzortzakis, D. Christofilos, and F. Vallee, "Nonequilibrium electron dynamics in noble metals," Phys. Rev. B **61,** 16956–16966 (2000).
15. E. Colavita, A. Franciosi, C. Mariani, and R. Rosei, "Thermoreflectance test of W, Mo, and paramagnetic Cr band structures," Phys. Rev. B **27,** 4684–4693 (1983).
16. J. Hanus, J. Feinleib, and W. J. Scouler, "Low-energy interband transitions and band structure in nickel," Phys. Rev. Lett. **19,** 16–20 (1967).
17. H. Ehrenreich, H. R. Philipp, and D. J. Olenchna, "Optical properties and Fermi surface of nickel," Phys. Rev. **131,** 2469–2477 (1963).
18. J. W. D. Connolly, "Energy bands in ferromagnetic nickel," Phys. Rev. **159,** 415–426 (1967).
19. F. Weiling and J. Callaway, "Semiempirical description of energy bands in nickel," Phys. Rev. B **26,** 710–719 (1982).
20. J. C. Phillips, "Fermi surface of ferromagnetic nickel," Phys. Rev. **133,** A1020–A1028 (1964).
21. E. Beaurepaire, J.-C. Merle, A. Daunois, and J.-Y. Bigot, "Ultrafast spin dynamics in ferromagnetic nickel," Phys. Rev. Lett. **76,** 4250–4253 (1996).
22. B. Koopmans, M. van Kampen, J. T. Kohlhepp, and W. J. M. de Jonge, "Femtosecond spin dynamics of epitaxial Cu(111)/Ni/Cu wedges," Appl. Phys. Lett. **87,** 5070–5072 (2000).
23. L. Guidoni, E. Beaurepaire, and J.-Y. Bigot, "Magneto-optics in the ultrafast regime: thermalization of spin populations in ferromagnetic films," Phys. Rev. Lett. **89,** 017401 (2002).
24. J. Gudde, U. Conrad, V. Jahnke, J. Hohlfeld, and E. Matthias, "Magnetization dynamics of Ni and Co films on Cu(001) and of bulk nickel surfaces," Phys. Rev. B **59,** R6608–R6611 (1999).
25. I. H. Chowdhury and X. Xu, "Heat transfer in femtosecond laser processing of metal," Numer. Heat Transfer Part A **44,** 219–232 (2003).
26. T. Q. Qiu and C. L. Tien, "Heat transfer mechanisms during short-pulse laser heating of metals," J. Heat Transfer **115,** 835–841 (1993).
27. C. A. C. Bosco, A. Azevedo, and L. H. Acioli, "Substrate dependent ultrafast dynamics in thin NiFe films," Appl. Phys. Lett. **83,** 1767–1769 (2003).
28. T. Q. Qiu and C. L. Tien, "Size effects on nonequilibrium laser heating of metal films," J. Heat Transfer **115,** 842–847 (1993).
29. A. N. Smith, J. L. Hostetler, and P. M. Norris, "Nonequilibrium heating in metal films: an analytical and numerical analysis," Numer. Heat Transfer Part A **35,** 859–873 (1999).
30. T. Q. Qiu and C. L. Tien, "Heat transfer mechanisms during short-pulse laser heating on metals," in *Transport Phenomena in Materials Processing and Manufacturing* (ASME, 1992), HTD-Vol. 196, pp. 41–49.
31. S. I. Anisimov, B. L. Kapeliovich, and T. L. Perel'man, "Electron emission from metal surfaces exposed to ultrashort laser pulses," Sov. Phys. JETP **39,** 375–377 (1974).
32. N. K. Sherman, F. Brunel, P. B. Corkum, and F. A. Hegmann, "Transient response of metals to ultrashort pulse excitation," Opt. Eng. **28,** 1114–1121 (1989).
33. D. S. Ivanov and L. V. Zhigilei, "Combined atomistic-continuum modeling of short-pulse laser melting and disintegration of metal films," Phys. Rev. B **68,** 064114 (2003).
34. C. Kittel, *Introduction to Solid State Physics* (Wiley, 1996).
35. A. P. Caffrey, P. E. Hopkins, J. M. Klopf, and P. M. Norris, "Thin film non-noble transition metal thermophysical properties," Microscale Thermophys. Eng. **9,** 365–377 (2005).
36. D. E. Gray, *American Institute of Physics Handbook* (McGraw Hill, 1972).
37. F. Abeles, "Optics of thin films" in *Advanced Optical Techniques,* A. C. S. V. Heel, ed. (North-Holland, 1967), pp. 145–188.
38. R. Rosei and D. W. Lynch, "Thermomodulation spectra of Al, Au, and Cu," Phys. Rev. B **5,** 3883–3894 (1972).
39. S. D. Brorson, A. Kazeroonian, J. S. Moodera, D. W. Face, T. K. Cheng, E. P. Ippen, M. S. Dresselhaus, and G. Dresselhaus, "Femtosecond room-temperature measurement of the electron–phonon coupling constant λ in metallic superconductors," Phys. Rev. Lett. **64,** 2172–2175 (1990).
40. H. Hirori, T. Tachizaki, O. Matsuda, and O. B. Wright, "Electron dynamics in chromium probed with 20-fs optical pulses," Phys. Rev. B **68,** 113102 (2003).
41. W. J. Scouler, "Temperature-modulated reflectance of gold from 2 to 10 eV," Phys. Rev. Lett. **18,** 445–448 (1967).
42. R. J. Stevens, A. N. Smith, and P. M. Norris, "Signal analysis and characterization of experimental setup for the transient thermoreflectance technique," Rev. Sci. Instrum. **77,** 084901 (2006).
43. A. Brodeur and S. L. Chin, "Ultrafast white-light continuum generation and self-focusing in transparent condensed media," J. Opt. Soc. Am. B **16,** 637–650 (1999).
44. E. D. Palik, *Handbook of Optical Constants of Solids* (Academic, 1985).
45. N. W. Ashcroft and N. D. Mermin, *Solid State Physics* (Saunders College, 1976).
46. H. Enrenreich, H. R. Philipp, and D. J. Olenchna, "Optical properties and Fermi surface of nickel," Phys. Rev. **131,** 2469–2477 (1963).
47. J. W. C. de Vries, "Temperature-dependent resistivity measurements on polycrystalline SiO_2-covered thin nickel films," Thin Solid Films **150,** 209–215 (1987).
48. S.-S. Wellershoff, J. Gudde, J. Hohlfeld, J. G. Muller, and E. Matthias, "The role of electron–phonon coupling in femtosecond laser damage of metals," in Proc. SPIE **3343,** 378–387 (1998).
49. J. K. Chen, W. P. Latham, and J. E. Beraun, "The role of electron–phonon coupling in ultrafast laser heating," J. Laser Appl. **17,** 63–68 (2005).